

# Highly accelerated 3D dynamic contrast enhanced MRI from sparse spiral sampling using integrated partial separability model and JSENSE

Jingyuan Lyu <sup>a</sup>, Pascal Spincemaille <sup>b</sup>, Yi Wang <sup>b</sup>, Yihang Zhou <sup>a</sup>, Fuquan Ren <sup>a</sup>, Leslie Ying <sup>\*a</sup>

<sup>a</sup> Department of Biomedical Engineering, Department of Electrical Engineering,  
The State University of New York at Buffalo, Buffalo, New York, USA

<sup>b</sup> Department of Radiology, Weill Cornell Medical College, New York, New York, USA

## ABSTRACT

Dynamic contrast enhanced MRI requires high spatial resolution for morphological information and high temporal resolution for contrast pharmacokinetics. The current techniques usually have to compromise the spatial information for the required temporal resolution. This paper presents a novel method that effectively integrates sparse sampling, parallel imaging, partial separable (PS) model, and sparsity constraints for highly accelerated DCE-MRI. Phased array coils were used to continuously acquire data from a stack of variable-density spiral trajectory with a golden angle. In reconstruction, the sparsity constraints, the coil sensitivities, spatial and temporal bases of the PS model are jointly estimated through alternating optimization. Experimental results from in vivo DCE liver imaging data show that the proposed method is able to achieve high spatial and temporal resolutions at the same time.

**Keywords:** dynamic contrast enhanced MRI, partial separable model, parallel imaging, coil sensitivity, JSENSE, sparsity.

## 1. INTRODUCTION

Dynamic contrast-enhanced magnetic resonance imaging (DCE-MRI) has provided a collection of sequential sets of morphological images. These MRI “movies” represent a potentially major development in the management of a wide range of diseases and have particular applicability in oncology<sup>1</sup>. Variations in microvascular structure and pathophysiology give rise to spatiotemporal variation in enhancement patterns that can reveal valuable physiological properties such as capillary surface area, blood flow, endothelial permeability, and the size of the extravascular space in which contrast is distributed<sup>2</sup>. These properties can be used to identify ongoing biological processes required for non-invasive diagnosis.

Although DCE-MRI has already been used clinically, its practical impact is still limited by the relatively low spatiotemporal resolution<sup>3</sup>. DCE-MRI demands high spatial resolution to fully characterize the morphological information and high temporal resolution to fully characterize the contrast pharmacokinetics. In the existing DCE-MRI methods, the spatial resolution has to be compromised for the required temporal resolution<sup>4</sup>.

A number of methods<sup>5-12</sup> have been proposed to improve the spatiotemporal resolution of dynamic imaging by highly undersampling the MRI data in  $(k,t)$  space and reconstructing the image using spatial, temporal or both constraints. When combined with other fast imaging techniques, such as fast scanning and parallel imaging, these methods hold promise for even higher spatiotemporal resolution. Some recent works<sup>13-15</sup> have investigated combination of non-Cartesian trajectories, parallel imaging, and compressed sensing for fast dynamic imaging.

In this paper, we propose a novel method to effectively integrate spiral acquisition, parallel imaging, partial separable (PS) model, and sparse constraints for highly accelerated dynamic contrast enhanced MRI. In data acquisition, the proposed method exploits 3D spiral trajectories with golden angle. In image reconstruction, the coil sensitivities, spatial and temporal bases of the PS model are jointly estimated through alternating optimization. Experimental results from in vivo DCE liver imaging data demonstrate the proposed method is able to achieve high spatiotemporal resolution.

## 2. PROPOSED METHOD

### 2.1. Problem formulation

The main goal of the proposed method is to recover the dynamic image sequence  $\gamma(\mathbf{x}, t)$  from its under-sampled Fourier measurements acquired through multiple channels of a phased array coil, where  $x$  and  $t$  represent spatial location and time respectively. The sequence can be represented as the  $M \times N$  Casorati matrix:

$$\Gamma_{M \times N} = \begin{pmatrix} \gamma(x_1, t_1) & \cdots & \gamma(x_1, t_N) \\ \gamma(x_2, t_1) & \cdots & \gamma(x_2, t_N) \\ \cdot & \cdots & \cdot \\ \gamma(x_M, t_1) & \cdots & \gamma(x_M, t_N) \end{pmatrix} \in \mathbf{C}^{M \times N} \quad (1)$$

Here,  $M$  is the number of voxels in the image and  $N$  is the number of image frames in the dataset. The columns of  $\Gamma$  correspond to the voxels of each time frame. Assuming that  $D$  samples are acquired in k-space from each channel at each time, the imaging equation can be written as:

$$\mathbf{d}_\ell = \mathbf{F}(\mathbf{S}_\ell \bullet \Gamma) + \mathbf{e}_\ell, \quad (2)$$

where  $\mathbf{d}_\ell \in \mathbf{C}^{D \times N}$  and  $\mathbf{e}_\ell \in \mathbf{C}^{D \times N}$  are the measured data matrix in  $(k, t)$  space and noise matrix at the  $\ell$ -th channel respectively;  $\mathbf{F}$  is the 2D Fourier matrix which depends on the sampling trajectory;  $\mathbf{S}_\ell$  is the sensitivity matrix of the  $\ell$ -th channel in spatial and temporal domain which has the same form as Eq. (1);  $\bullet$  denotes the element-wise product. The measured data from all channels can be combined together to form the complete imaging equation that represents the entire encoding process in space, sensitivity, and time. In highly accelerated dynamic imaging, Eq. (2) is highly underdetermined and thus solving Eq. (2) for  $\Gamma$  is highly ill-posed. In order to address the issue of ill-posedness, we exploit the following model and constraints.

#### A. PS model on dynamic image sequence

The PS model assumes  $\gamma(\mathbf{x}, t)$  to be spatial-temporal partially separable<sup>7, 16, 17</sup>. Then  $\Gamma$  can be represented as the product of a spatial coefficient matrix  $\mathbf{U}_s$  and a temporal basis  $\mathbf{V}_t$ :

$$\Gamma^{M \times N} = \mathbf{U}_s^{M \times R} \mathbf{V}_t^{R \times N}, \quad (3)$$

where  $R$  is the order of the PS model, or rank of  $\Gamma$ . The PS model is able to capture spatial-temporal correlation often observed in dynamic image sequences. The higher the order  $R$  is, the less the spatial-temporal correlation is present in the image sequence.

#### B. Sparse constraint on temporal frequency

We further assume the dynamic image sequences present slow variations in time<sup>10, 17</sup>. Therefore the signal in the spatial and temporal frequency domain is sparse. That is,  $\Gamma \mathbf{F}_t$  has very few significant elements, where  $\mathbf{F}_t$  represents the temporal Fourier transform.

#### C. Polynomial model on coil sensitivities

In parallel imaging, accurate coil sensitivities are usually needed implicitly or explicitly in reconstruction. To ensure accurate sensitivities are used in reconstruction, the sensitivity functions are regarded as unknowns to be estimated during the reconstruction process. We assume the coil sensitivity information is varying with the image sequence at different time instants. As a result, each time frame entails different sensitivity maps and thereby for the  $\ell$ -th channel, we have

$$\mathbf{S}_\ell = [\mathbf{s}_\ell(t_1), \mathbf{s}_\ell(t_2), \dots, \mathbf{s}_\ell(t_N)] \in \mathbf{C}^{M \times N} \quad (4)$$

We further assume the coil sensitivities are smooth spatially and employ a polynomial parametric model for the coil sensitivity at each channel and each time<sup>18</sup>:

$$s_\ell(t_n) = \text{vec} \left[ \sum_{p=0}^K \sum_{q=0}^K a_{\ell,n}(p,q) (x - \bar{x})^p (y - \bar{y})^q \right] \quad (5)$$

where  $(x, y)$  denotes the location of a pixel,  $(\bar{x}, \bar{y})$  denotes the averaged location, and  $a_{\ell,n}(p, q)$  is the coefficient of a polynomial for a specific channel and time. With the coefficient vector  $\mathbf{a}_\ell$  of the  $\ell$ -th channel explicitly represented in the imaging equation, Eq. (2) can be rewritten as

$$\mathbf{d}_\ell = \mathbf{E}(\mathbf{a}_\ell)(\Gamma) + \mathbf{e}_\ell \quad (6)$$

Here,  $\mathbf{E}: \mathbf{C}^{M \times N} \rightarrow \mathbf{C}^{D \times N}$  represents an operator which integrates both the Fourier transform with a specified undersampling trajectory in  $(k, t)$ -space and the coil sensitivity modulation.

## 2.2. Image reconstruction algorithm

Incorporating the above models, the image reconstruction problem is formulated as

$$\min_{\mathbf{U}_s, \mathbf{V}_t, \mathbf{a}} \sum_{\ell=1}^C \|\mathbf{d}_\ell - \mathbf{E}(\mathbf{a}_\ell)(\mathbf{U}_s \mathbf{V}_t)\|_2^2 + \lambda \|\text{vec}(\mathbf{U}_s \mathbf{V}_t \mathbf{F}_t)\|_1 \quad (7)$$

where the  $L_1$  norm term enforces the sparsity constraint in spatial and temporal frequency domain.

### A. Initialization

#### Initial estimation of $\mathbf{V}_t$

An initial temporal basis is first estimated from the central densely sampled spiral k-space data within a chosen radius. Although the  $(k, t)$  space data is highly undersampled, the center k-space is still sampled with Nyquist rate with variable-density spiral trajectory. These data can be used to obtain a series of low spatial resolution but high temporal resolution images, represented in matrix  $\Gamma_{\text{LR}}$ . Then the temporal basis  $\mathbf{V}_t$  can be obtained from the  $R$  dominant right singular vectors through the singular value decomposition (SVD)<sup>7</sup>. Selection of  $R$  often needs to balance the representation capability of the model and the numerical condition of the resulting model fitting problem. When  $R$  is too low, the model may fail to capture some temporal features, although the corresponding model fitting problem is often well-conditioned. When  $R$  is too high, the model fitting problem becomes under determined, which can amplify modeling errors and increase computation complexity.

#### Initial estimation of sensitivity maps

The same central k-space data with Nyquist sampling density is used to estimate the coil sensitivity maps initially. These central k-space data after Fourier transform produces low-resolution reference images. To derive the sensitivities, these low-resolution reference images are divided by their sum-of squares (SoS) combination<sup>19</sup>.

### B. Alternating optimization

#### Updating the spatial basis $\mathbf{U}_s$

When the temporal basis  $\mathbf{V}_t$  and the sensitivity maps are estimated initially, we assume they are given and use the initial estimations to find  $\mathbf{U}_s$ . The problem is simplified to:

$$\hat{\mathbf{U}}_s = \arg \min_{\mathbf{U}_s} \sum_{\ell=1}^C \|\mathbf{d}_\ell - \mathbf{E}(\hat{\mathbf{a}}_\ell)(\mathbf{U}_s \hat{\mathbf{V}}_t)\|_2^2 + \lambda \|\text{vec}(\mathbf{U}_s \hat{\mathbf{V}}_t \mathbf{F}_t)\|_1, \quad (8)$$

and is solved using the majorize-minimize algorithm<sup>17</sup>.

### Updating $\mathbf{a}_\ell$

Since the second part in Eq. (7) is not related to the sensitivity maps, the following form is used to update  $\mathbf{a}_\ell$ :

$$\hat{\mathbf{a}}_\ell = \min_{\mathbf{a}_\ell} \|\mathbf{d}_\ell - \mathbf{E}(\mathbf{a}_\ell)(\hat{\mathbf{U}}_s \hat{\mathbf{V}}_t)\|_2^2, \text{ all } \ell \quad (9)$$

Since the polynomial model already incorporates the smoothness constraint, no regularization is needed on sensitivity functions. We choose the power of  $x$  and  $y$  to be the same (both equal to  $K$ , e.g.  $K=7$ ) and define it as the order of the polynomial. A low-order of  $K$  is sufficient, due to the smooth nature of coil sensitivity in general. As long as the order of the polynomial is not too high when compared to the number of data samples, the above least-squares problem is overdetermined and thus has a unique solution.

### Updating temporal basis $\mathbf{V}_t$

After the entire image sequence is recovered for the previous iteration, the high resolution images are used to perform SVD and update the temporal basis  $\mathbf{V}_t$ .

$$\hat{\mathbf{V}}_t = \arg \min_{\mathbf{V}_t} \sum_{\ell=1}^C \|\mathbf{d}_\ell - \mathbf{E}(\hat{\mathbf{a}}_\ell)(\hat{\mathbf{U}}_s \mathbf{V}_t)\|_2^2 + \lambda \|\text{vec}(\hat{\mathbf{U}}_s \mathbf{V}_t \mathbf{F}_t)\|_1$$

## 3. RESULTS

In this section, we show a set of representative results from *in vivo* real-time DCE liver MRI experiments to evaluate the performance of the proposed method. A 3D fast spoiled gradient echo stack of spirals sequence with partial Fourier slice encoding<sup>15</sup> was used for data acquisition (TR/TE=7.2/0.6 ms, FOV=340mm, slice thickness=5mm, matrix size = 256x256x36, 8 channel cardiac coil). Consecutive spiral leaves are rotated by the golden ratio angle of  $220^\circ$  such that each new spiral leaf is sampling a substantially different part of  $k$ -space compared to the immediately preceding leaf. For each spiral leaf, a full set of slice encodings (partially encoded) is acquired. A variable density spiral trajectory was used where 48 spirals fully sample the  $k_x$ - $k_y$  plane.

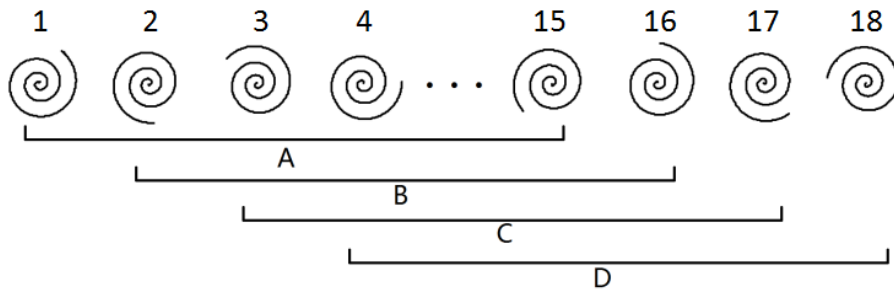


Figure 1. Sampling trajectory for each frame and schematic of sliding window. For example, A, B, C, and D represent the reference spiral leaves for Frame 8, 9, 10 and 11, respectively.

Fig. 1 illustrates how the sliding window method and the proposed method combine different leaves to obtain the undersampled or full  $k$ -space data for reconstruction. In sliding window, combining 48 leaves would satisfy the Nyquist sampling criterion spatially, but compromise the temporal resolution. In Fig. 2, we compare the results of the proposed method which combines 15 leaves with the results of the sliding window method which combines 15 and 48 leaves.

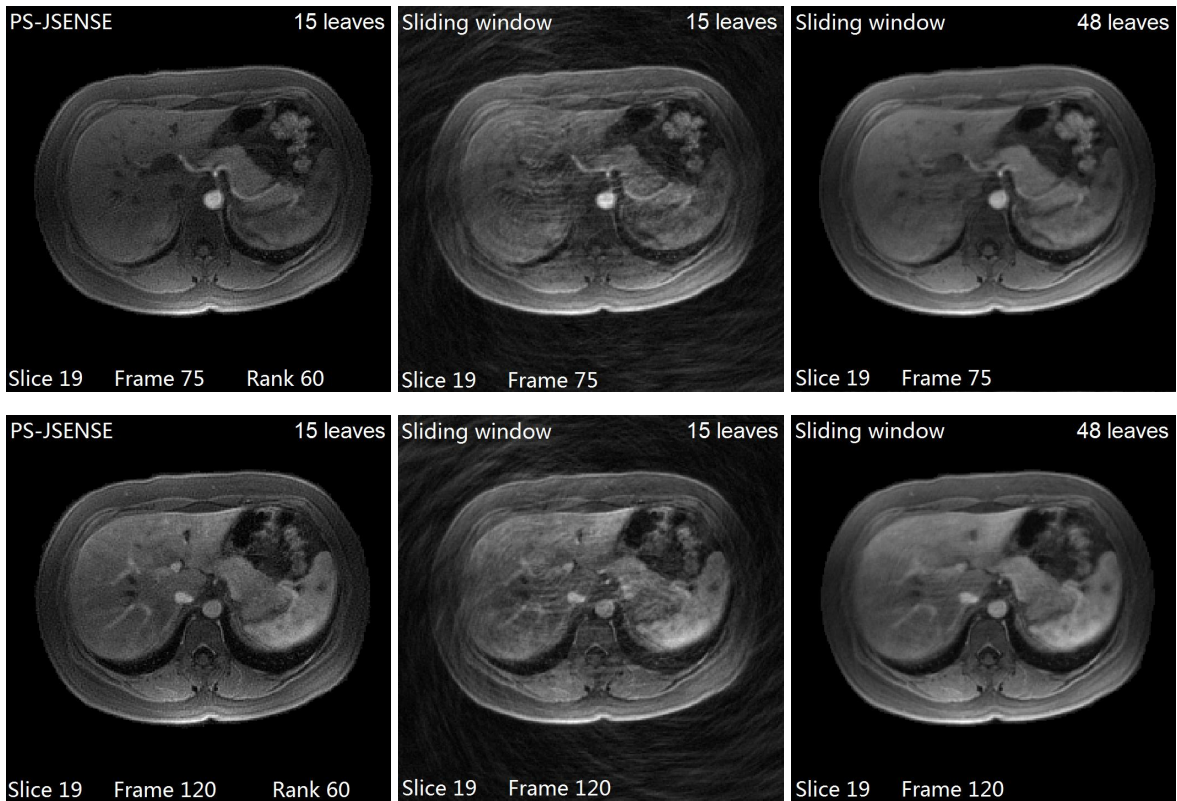


Figure 2. Reconstructions of the proposed method (left), sliding window method with 15 (middle) and 48 leaves (right).

From the results we can see that the proposed method is able to remove the aliasing artifacts in sliding window with 15 leaves (SW 15), and improve the spatial resolution in sliding window with 48 leaves (SW 48). The edges are sharp in the reconstructions from the proposed method.

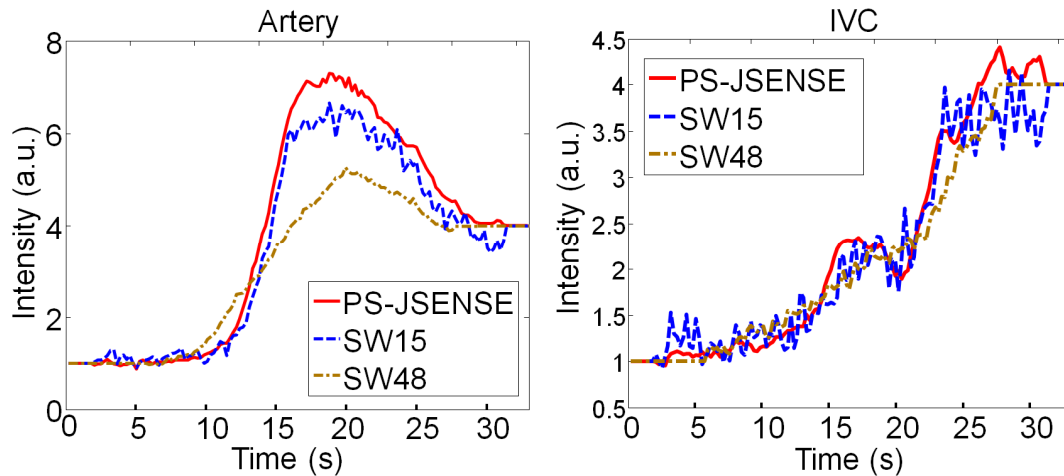


Figure 3. The intensity vs. temporal frame curves of artery and IVC for three different reconstructions.

The intensity curves of region of interest (ROI) for both methods are also compared. It is seen that the proposed method with 15 leaves is able to suppress the aliasing artifacts present in the sliding-window reconstruction with 15 leaves and achieve a better spatial resolution than the sliding-window reconstruction with 48 leaves. In addition, the small

respiratory motion causes artifacts in SW 48 but no artifacts in PS-JSENSE with 15 leaves. The intensity curves show that the proposed method is superior to the sliding-window method in preserving kinetic information.

#### 4. CONCLUSION

We have proposed a novel method to integrate parallel imaging, the PS model, and the sparsity constraint in the same framework. Our results using a liver DCE-MRI dataset demonstrate that the proposed method is able to balance the tradeoff between the spatial image quality and temporal resolution in DCE-MRI. The proposed method shows significant improvement over the conventional sliding window method.

#### REFERENCES

- [1] Taylor, J. S., and Reddick, W. E., "Evolution from empirical dynamic contrast-enhanced magnetic resonance imaging to pharmacokinetic MRI," *Adv. Drug Deliv. Rev.*, 41(1), 91-110 (2000).
- [2] Hayes, C., Padhani, A. R., and Leach, M.O., "Assessing changes in tumor vascular function using dynamic contrast-enhanced magnetic resonance imaging," *NMR Biomed.*, 15(2), 154-163 (2002).
- [3] Padhani, A. R., "Dynamic contrast-enhanced MRI in clinical oncology: current status and future directions," *J. Magn. Reson. Imaging*, 16(4), 407-422 (2002).
- [4] Krishnan, S., and Chenevert, T. L., "Spatio-temporal bandwidth-based acquisition for dynamic contrast-enhanced magnetic resonance imaging," *J. Magn. Reson. Imaging*, 20(1), 129-137 (2004).
- [5] Liang, Z.-P., and Lauterbur, P. C., "An efficient method for dynamic magnetic resonance imaging," *IEEE Trans. Med. Imag.*, 13(4), 677-686 (1994).
- [6] Madore, B., Glover, G. H., and Pelc, N. J., "Unaliasing by Fourier-encoding the overlaps using the temporal dimension (UNFOLD), applied to cardiac imaging and fMRI," *Magn. Reson. Med.*, 42(5), 813-828 (1999).
- [7] Liang, Z.-P., "Spatiotemporal imaging with partially separable functions," *Proc. IEEE Int. Symp. Biomed. Imag. (ISBI)*, Arlington, USA, 988-991 (2007).
- [8] Tsao, J., Boesiger, P., and Pruessmann, K. P., "k-t BLAST and k-t SENSE: dynamic MRI with high frame rate exploiting spatiotemporal correlations," *Magn. Reson. Med.*, 50(5), 1031-1042 (2003).
- [9] Lustig, M., Santos, J. M., Donoho, D. L., and Pauly, J. M., "k-t SPARSE: high frame rate dynamic MRI exploiting spatiotemporal sparsity," *Proc. 14th Annual Meeting ISMRM*, Seattle, USA, 2420 (2006).
- [10] Jung, H., Sung, K., Nayak, K. S., Kim, E. Y., and Ye, J. C., "k-t FOCUSS: A general compressed sensing framework for high resolution dynamic MRI," *Magn. Reson. Med.*, 61(1), 103-116 (2009).
- [11] Gamper, U., Boesiger, P., and Kozerke, S., "Compressed sensing in dynamic MRI," *Magn. Reson. Med.*, 59(2), 365-373 (2008).
- [12] Chen, L., Schabel, M. C., and DiBella, E. V. R., "Reconstruction of dynamic contrast enhanced magnetic resonance imaging of the breast with temporal constraints," *Magn. Reson. Imag.*, 28(5), 637-645 (2010).
- [13] Uecker, M., Zhang, S., Voit, D., Karaus, A., Merboldt, K. D., and Frahm, J., "Realtime MRI at a resolution of 20 ms," *NMR Biomed.* 23(8), 986-994 (2010).
- [14] Otazo, R., Kim, D., Axel, L. and Sodickson, D. K., "Combination of compressed sensing and parallel imaging for highly accelerated first-pass cardiac perfusion MRI," *Magn. Reson. Med.*, 64(3), 767-776 (2010).
- [15] Xu, B., Spincemaille, P., Chen, G., Agrawal, M., Nguyen, T. D., Prince, M. R. and Wang, Y., "Fast 3D contrast enhanced MRI of the liver using temporal resolution acceleration with constrained evolution reconstruction," *Magn. Reson. Med.*, 69(2), 370-381 (2013).
- [16] Haldar, J. P., and Liang, Z.-P., "Spatiotemporal imaging with partially separable functions: A matrix recovery approach," *Proc. IEEE Int. Symp. Biomed. Imag.*, 716-719 (2010).
- [17] Zhao, B., Haldar, J. P., Christodoulou, A. G., and Liang, Z.-P., "Image reconstruction from highly undersampled (k, t)-space data with joint partial separability and sparsity constraints," *IEEE Trans. Med. Imag.*, 31(9), 1809-1820 (2012).
- [18] Ying, L., and Sheng, J., "Joint image reconstruction and sensitivity estimation in SENSE (JSENSE)," *Magn. Reson. Med.*, 57(6), 1196-1202 (2007).
- [19] Sheng, J., Liu, B., and Ying, L., "Improved self-calibrated spiral parallel imaging using JSENSE," *Medical Engineering and Physics*, 31(5), 510-514 (2009).